Check for updates

American Society of Hematology
2021 L Street NW, Suite 900,
Washington, DC 20036
Phone: 202-776-0544 | Fax 202-776-0545
editorial@hematology.org

A zinc transporter, transmembrane protein 163 (TMEM163), is critical for the biogenesis of platelet dense granules

Tracking no: BLD-2020-007389R2

Yefeng Yuan (Beijing Key Laboratory for Genetics of Birth Defects; MOE Key Laboratory of Major Diseases in Children, Center for Medical Genetics, Beijing Pediatric Research Institute, Beijing Children's Hospital, China) Teng Liu (Beijing Tongren Hospital, Capital Medical University, China) Xiahe Huang (Institute of Genetics and Developmental Biology, Chinese Academy of Sciences, China) Yuanying Chen (Beijing Children's Hospital, China) Weilin Zhang (Institute of Zoology, Chinese Academy of Sciences, China) Ting Li (Institute of Genetics and Developmental Biology, Chinese Academy of Sciences, China) lin Yang (Institute of Genetics and Developmental Biology, Acdamy of Sciences of China., China) Quan Chen (Nankai University, China) Yingchun Wang (Institute of Genetics and Developmental Biology, Chinese Academy of Sciences, China) Aihua Wei (Beijing Tongren Hospital, Capital Medical University, China) Wei Li (Beijing Children's Hospital, China)

Abstract:
Lysosome-related organelles (LROs) are a category of secretory organelles enriched with ions such as Ca^{2+}, which are maintained by ion transporters or channels. Homeostasis of these ions is important for LRO biogenesis and secretion. Hermansky-Pudlak syndrome (HPS) is a recessive disorder with defects in multiple LROs, typically platelet dense granules (DGs) and melanosomes. However, the underlying mechanism of DG deficiency is largely unknown. Using quantitative proteomics, we identified a previously unreported platelet Zn^{2+} transporter TMEM163, which was significantly reduced in BLOC-1 (*Dtnbp1* ^{sdy} and *Pldn* ^{pa}), BLOC-2 (*Hps6* ^{ru}) or AP-3 (*Ap3b1* ^{pe}) deficient mice and HPS patients (HPS2, 3, 5, 6, or 9). We observed similar platelet DG defects and abnormal intracellular zinc accumulation in platelets of mice deficient in either TMEM163 or dysbindin (a BLOC-1 subunit). In addition, we discovered that BLOC-1 was required for the trafficking of TMEM163 to perinuclear DG and late endosome (LE) marker-positive compartments (likely DG precursors) in MEG-01 cells. Our results suggest that TMEM163 is critical for DG biogenesis and BLOC-1 is required for the trafficking of TMEM163 to putative DG precursors. These new findings suggest that loss of TMEM163 function results in disruption of intracellular zinc homeostasis, and provide insights into the pathogenesis of HPS or platelet storage pool deficiency.

Conflict of interest: No COI declared

COI notes:

Preprint server: No;

Author contributions and disclosures: Y.Y. and W.L. designed the research, analyzed the data and wrote the manuscript. Y.Y. performed most of the experiments; T.Liu and A.W. recruited all the subjects and collected the written informed consents; Y.C. participated in Tmem163-KO mouse generation; W.Z. and Q.C. assisted in the design of platelet aggregation assays; T.Li provided technical support for flow cytometry; L.Y. provided technical support for electron microscopy; X.H. and Y.W. helped to analyze mass spectrometry data.

Non-author contributions and disclosures: Yes; Prof. Richard T. Swank from Roswell Park Cancer Institute (Buffalo, NY) proofread this manuscript for improving English writing.

Agreement to Share Publication-Related Data and Data Sharing Statement: Details on methods can be requested from Dr. Wei Li, liwei@bch.com.cn.

Clinical trial registration information (if any):

Downloaded from http://ashpublications.org/blood/article-pdf/doi/10.1182/blood.2020007389/1799023/blood.2020007389.pdf by guest on 30 January 2021

A zinc transporter, transmembrane protein 163 (TMEM163), is critical for the biogenesis of platelet dense granules

Yefeng Yuan [1, 2], Teng Liu [3, 4], Xiahe Huang [2], Yuanying Chen [1], Weilin Zhang [5], Ting Li [2], Lin Yang [2], Quan Chen [5, 6], Yingchun Wang [2], Aihua Wei [3] and Wei Li [1, 4] *

[1] Beijing Key Laboratory for Genetics of Birth Defects, Beijing Pediatric Research Institute; MOE Key Laboratory of Major Diseases in Children; Genetics and Birth Defects Control Center, National Center for Children's Health; Beijing Children's Hospital, Capital Medical University, Beijing 100045, China

[2] University of Chinese Academy of Sciences, Institute of Genetics and Developmental Biology, Chinese Academy of Sciences, Beijing 100101, China

[3] Department of Dermatology, Beijing Tongren Hospital, Capital Medical University, Beijing 100730, China

[4] Shunyi Women and Children's Hospital of Beijing Children's Hospital, Beijing 101300, China

[5] State Key Laboratory of Membrane Biology, Institute of Zoology, Chinese Academy of Sciences, Beijing 100101, China

[6] Tianjin Key Laboratory of Protein Science, College of Life Sciences, Nankai University, Tianjin 300071, China

* Correspondence to Dr. Wei Li, Beijing Children's Hospital, Capital Medical University, 56 Nan Li Shi Road, Xicheng District, Beijing 100045, China; Tel: +86-10-5961 6628, E-mail: liwei@bch.com.cn.

Running Title: *TMEM163 in platelet dense granules.*

Downloaded from http://ashpublications.org/blood/article-pdf/doi/10.1182/blood.2020007389/1799023/blood.2020007389.pdf by guest on 30 January 2021

Key Points

- A zinc transporter, TMEM163, is essential for the biogenesis and function of platelet dense granules (DGs).
- BLOC-1 complex is involved in the trafficking of TMEM163 to platelet DGs which explains the defective DGs in Hermansky-Pudlak syndrome.

Abstract

Lysosome-related organelles (LROs) are a category of secretory organelles enriched with ions such as Ca^{2+}, which are maintained by ion transporters or channels. Homeostasis of these ions is important for LRO biogenesis and secretion. Hermansky-Pudlak syndrome (HPS) is a recessive disorder with defects in multiple LROs, typically platelet dense granules (DGs) and melanosomes. However, the underlying mechanism of DG deficiency is largely unknown. Using quantitative proteomics, we identified a previously unreported platelet Zn^{2+} transporter TMEM163, which was significantly reduced in BLOC-1 (*Dtnbp1* ^{sdy} and *Pldn* ^{pa}), BLOC-2 (*Hps6* ^{ru}) or AP-3 (*Ap3b1* ^{pe}) deficient mice and HPS patients (HPS2, 3, 5, 6, or 9). We observed similar platelet DG defects and abnormal intracellular zinc accumulation in platelets of mice deficient in either TMEM163 or dysbindin (a BLOC-1 subunit). In addition, we discovered that BLOC-1 was required for the trafficking of TMEM163 to perinuclear DG and late endosome (LE) marker-positive compartments (likely DG precursors) in MEG-01 cells. Our results suggest that TMEM163 is critical for DG biogenesis and BLOC-1 is required for the trafficking of TMEM163 to putative DG precursors. These new findings suggest that loss of TMEM163 function results in disruption of intracellular zinc homeostasis, and provide insights into the pathogenesis of HPS or platelet storage pool deficiency.

Downloaded from http://ashpublications.org/blood/article-pdf/doi/10.1182/blood.2020007389/1799023/blood.2020007389.pdf by guest on 30 January 2021

Introduction

HPS is a recessive disorder, featured by oculocutaneous albinism, prolonged bleeding, and ceroid deposition. It is also accompanied by lung fibrosis, colitis, and other complications in some cases. [1,2] The characteristic hallmarks of HPS are defects in multiple lysosome-related organelles (LROs), including dense granules (DGs) in platelets, melanosomes in melanocytes, Weibel-Palade bodies in endothelial cells, large-dense core vesicles in adrenal chromaffin cells, synaptic vesicles in neurons and lamellar bodies in alveolar type II epithelial cells. [2-6] LROs are regarded as a category of secretory organelles sharing properties with conventional lysosomes, such as highly glycosylated integral lysosome-associated membrane proteins (LAMPs) and enrichment of intralumenal ions such as Ca^{2+}. [2,3,7]

As inferred from melanosome biogenesis studies, platelet DGs are thought to originate via intermediary endosomes and multivesicular bodies (MVBs), and proteins may be transported to immature or mature DGs by a variety of protein complexes, such as the HPS protein associated complexes (HPACs). [2,8-14] However, the underlying mechanisms whereby HPACs affect DG biogenesis remain uncharacterized. In addition, Rab32 and Rab38 regulate the transport of LAMP2 and VMAT2 (DG integral membrane protein) from early endosomes to mepacrine positive compartments.[10,15] The Rab32 and Rab38 double mutant mimics severe HPS and has decreased DGs.[16] Rab32/Rab38 may not directly interact with these cargoes (e.g. LAMP2 or VMAT2), and whether LAMP2 or VMAT2 deficiency causes defective DG biogenesis is unknown. Deficiency of SLC35D3 (a transmembrane protein) affects DG biogenesis, [17,18] but there is no clear evidence that SLC35D3 is localized to DGs. Altogether,

Downloaded from http://ashpublications.org/blood/article-pdf/doi/10.1182/blood.2020007389/1799023/blood.2020007389.pdf by guest on 30 January 2021

the underlying mechanisms of DG biogenesis are largely unknown.

Traditionally, ion channels play a pivotal role in LRO biogenesis. Two-pore channel 2 (TPC2) regulates the pH, release of Ca^{2+}, membrane dynamics and content exchange of mepacrine positive compartments in MEG-01 cells. [19] In melanocytes, TPC2 regulates melanosomal pH and size by mediating Ca^{2+} release from melanosomes, thus controlling pigmentation. [20] Our recent studies demonstrated that mitochondrial NCKX5 (a member of the K^+-dependent Na^+/Ca^{2+} exchanger family (NCKX) participates in melanosome maturation and pigment production by regulating Ca^{2+} homeostasis of melanosomes. [21] Thus, similar to the melanosome, homeostasis of lumenal ions is important for DG biogenesis. However, knowledge of ion transporters in DGs is very limited.

Rats have an increased bleeding tendency upon maintenance on a Zn^{2+} deficient diet. [22-24] In addition, a bleeding tendency along with abnormal platelet aggregation was noted in two cancer patients, one with squamous cell carcinoma and another with non-Hodgkin's lymphoma, presenting with a nutritional Zn^{2+} deficiency. Normal bleeding times and platelet aggregation were restored by dietary zinc supplementation. [25] Zn^{2+} is known as a mediator of hemostasis. [26-30] Upon incubation with exogenous Zn^{2+}, platelets stained with the fluorescent zinc indicator, FluoZin™-3, display a rapid fluorescence increase, [31] indicating that platelet Zn^{2+} entry pathways exist. It has been reported that intracellular zinc homeostasis is maintained by two highly conserved zinc transporter protein families, ZIP (SLC39) and ZNT (SLC30), in mammalian cells. The 14 members of ZIP protein family regulate influx of zinc into the cytoplasm from the extracellular matrix and from the lumen of vesicular compartments. By contrast, the 10 members of ZNT protein family regulate efflux of zinc

Downloaded from http://ashpublications.org/blood/article-pdf/doi/10.1182/blood.2020007389/1799023/blood.2020007389.pdf by guest on 30 January 2021

into the extracellular matrix and into the lumen of vesicular compartments from the cytoplasm. [32-39] However, there is no report of Zn^{2+}-selective ion channels or transporters in platelets. Zn^{2+} has been proposed as an intracellular second messenger, analogous to Ca^{2+}, being released into the cytosol from intracellular storage pools. [40] However, the storage pools of Zn^{2+} in platelets have not been resolved.

In rat brain synaptosomes, transmembrane protein 163 (TMEM163), also called synaptic vesicle 31 (SV31), was first identified as a synaptic vesicle membrane protein binding zinc. [41] Exogenously expressed rodent TMEM163 mainly localized to the plasma membrane, lysosomes and synaptic vesicles. [42-44] Purified rodent TMEM163 reconstituted in lipid bilayers assembles into a dimer and functions as a proton-dependent Zn^{2+} transporter. [45] In addition, TMEM163 interacts with transient receptor potential mucolipin-1 (TRPML1), which has been implicated in mucolipidosis type IV (MLIV) pathogenesis. Both fibroblasts of a MLIV patient and human embryonic kidney (HEK293) cells with knock-down of TRPML1 showed abnormal lysosomal zinc accumulation. [43,44,46] Furthermore, TRPML1-deficient mice displayed increased zinc levels in postmortem brain, [46] suggesting that TRPML1 and TMEM163 play critical roles in intracellular zinc homeostasis. In the Indian population, TMEM163 is a GWAS candidate gene associated with insulin resistance and type 2 diabetes. [47] Although TMEM163 transcripts are detected in numerous tissues, including brain, kidney, lung, pancreas, testis and ovary, [41,43] The function of TMEM163 is controversial, [43,48] and its presence, localization and function in platelets are unknown.

In the present study, we find that TMEM163 is a critical component of the limiting membrane of the DG and the late endosome (LE) marker-positive compartment (likely

Downloaded from http://ashpublications.org/blood/article-pdf/doi/10.1182/blood.2020007389/1799023/blood.2020007389.pdf by guest on 30 January 2021

precursor of DG) in MEG-01 cells. TMEM163 is reduced in platelets of mice and HPS patients lacking the HPACs (BLOC-1, BLOC-2 and AP-3). We demonstrate that BLOC-1 interacts with TMEM163 during its transport from early endosomes to perinuclear DG and LE marker-positive compartments. This may explain the similar DG defects in both *Tmem163* knockout mice and in some of the above-mentioned HPS mutant mice.

Materials and Methods

Mice

The sandy (*Dtnbp1* ^{sdy}) mutant in the C57BL/6J background (wild-type) was originated from *sdy* mutant in the DBA/2J background [49] through backcrossing at least 8 generations. Other mouse mutants and their controls including pallid (*Pldn* ^{pa}), ruby-eye (*Hps6* ^{ru}), pale-ear (*Hps1* ^{ep}), pearl (*Ap3b1* ^{pe}), buff (*Vps33a* ^{bf}), a double mutant of ruby-eye and pale-ear (*ru/ep*) and a double mutant of buff and pale-ear (*bf/ep*) in the C57BL/6J background were derived as described previously. [5,50] They were obtained from Prof. Richard T. Swank's laboratory at Roswell Park Cancer Institute (Buffalo, New York, USA). The *Tmem163* knockout mice (*Tmem163-KO*) were generated using Biosset's EGE system based on CRISPR/Cas9 in the C57BL/6J background. To ensure the genotypes of the littermates, PCR amplifications were designed according to the targeted deletion of exons 1-2. All mice in this study were bred in the animal facility of the Institute of Genetics and Developmental Biology (IGDB), Chinese Academy of Sciences. All procedures were approved by the Institutional Animal Care and Use Committee of IGDB. Age matched wild-type mice (C57BL/6J, B6) or heterozygous mice were used as background controls.

Downloaded from http://ashpublications.org/blood/article-pdf/doi/10.1182/blood.2020007389/1799023/blood.2020007389.pdf by guest on 30 January 2021

Human subjects

The twelve HPS1~HPS6 patients (3 HPS1, 1 HPS2, 2 HPS3, 1 HPS4, 2 HPS5, 3 HPS6) were identified in our group, and their clinical features and genotypes were described previously.[51] One HPS9 patient was identified recently (Liu, et al. in press). Their parents were recruited in this study as controls. This study was approved by the internal review board of the bioethics committees of Beijing Tongren Hospital and Beijing Children's Hospital, Capital Medical University. The study followed the Declaration of Helsinki. Informed consent was signed by all subjects participating in this study. 2 mL peripheral blood samples were collected from all subjects for enrichment of platelets for immunoblotting.

Data analysis

All data were obtained from at least three independent experiments and expressed as mean ± SEM. All the quantitative results were plotted by one-way ANOVA with Tukey's post-test, except where specified otherwise such as the Student's *t*-test. Error bars indicate SEM. $*P < 0.05$; $**P < 0.01$; $***P < 0.001$; N.S., not significant. All graphs were drawn in GraphPad Prism 5 (La Jolla, CA, USA).

Supplementary Materials and Methods

Details of additional materials and methods can be found in the online Supplemental Data file.

Downloaded from http://ashpublications.org/blood/article-pdf/doi/10.1182/blood.2020007389/1799023/blood.2020007389.pdf by guest on 30 January 2021

Results

TMEM163 expression in platelets is reduced in murine mutants and human patients of HPS protein associated complexes BLOC-1, BLOC-2 and AP-3

To investigate how HPACs function in DG biogenesis, we isolated the platelets of sandy (*sdy,* deficiency in BLOC-1 subunit dysbindin) and its heterozygous littermates ($sdy^{+/-}$) for mass spectrometry. Using quantitative proteomics, we identified an uncharacterized transmembrane protein TMEM163 (SV31) that was decreased in *sdy* mice compared with $sdy^{+/-}$ mice. This protein is similar to CD63 (one type of DG integral membrane proteins) (Figure 1A, B, Supplemental Table 1, Supplemental Figure 1). To verify the mass spectrometry results, we quantified endogenous TMEM163 protein expression in platelet lysates from *sdy* and $sdy^{+/-}$ mice by immunoblotting (Figure 1C). For comparison, we measured other lysates of platelets from BLOC-1-deficient pallid (*pa*) (Figure 1D), BLOC-2-deficient ruby-eye (*ru*) (Figure 1E), AP-3-deficient pearl (*pe*) (Figure 1F), double mutant of ruby-eye and pale-ear (*ru/ep*) (Figure 1I) and their littermate control mice. BLOC-1, BLOC-2 and AP-3 mutants showed significant reduction of TMEM163 relative to their littermate control mice (Figure 1K). Interestingly, reduced TMEM163 in BLOC-1-, BLOC-2- and AP-3-deficient platelets is similar to observations of reduced SLC35D3 in these mutant mice,[17] suggesting that both TMEM163 and SLC35D3 are likely transported by these HPACs. However, lysates of BLOC-3-deficient pale-ear (*ep*) (Figure 1G), buff (*bf*) with the $VPS33A^{D251E}$ mutation (Figure 1H) and double mutant of buff and pale-ear (*bf/ep*) (Figure 1J) showed no alteration of TMEM163 expression (Figure 1K). Consistently, one case of a BLOC-1 deficient patient (1 HPS9), seven cases of

Downloaded from http://ashpublications.org/blood/article-pdf/doi/10.1182/blood.2020007389/1799023/blood.2020007389.pdf by guest on 30 January 2021

BLOC-2 deficient patients (2 HPS3, 2 HPS5, 3 HPS6) and one case of an AP-3 deficient patient (1 HPS2) showed significant reduction of TMEM163 relative to the healthy controls (Figure 1L-N). However, four cases of BLOC-3 deficient patients (3 HPS1, 1 HPS4) showed no alteration of TMEM163 expression (Figure 1M, N). These results agree with the finding that BLOC-1, BLOC-2 and AP-3 regulate cargo transport from endosomes to melanosomes in the same cargo-transport pathways in melanocytes, [11,12,50,52-55] whereas BLOC-3 and HOPS are involved in different routes in LRO biogenesis. [56] Altogether, these results indicate that TMEM163 may function in platelets, and that BLOC-1, BLOC-2 and AP-3 may regulate the transport of TMEM163 to platelet LROs.

TMEM163 localizes to perinuclear DG and LE marker-positive compartments and early endosome-like organelles

Platelet alpha granules (AGs) and dense granules (DGs) are two major types of intracellular organelles which belong to the LRO family. [9] Due to lack of an applicable antibody for endogenous TMEM163 immunofluorescence staining, we used a human megakaryocytic cell line, MEG-01 to determine the localization of TMEM163. [8,10] MEG-01 cells were simultaneously transfected with different tagged-TMEM163 constructs (Supplemental Figure 2), and we monitored Pearson correlation coefficients (PCCs) for the colocalization with multiple organelle markers. Confocal fluorescence microscopy revealed a high proportion of TMEM163 colocalization with platelet DG markers (Cherry-VMAT2, GFP-VMAT2, mepacrine and CD63) (PCCs, 0.74 ± 0.04, 0.76 ± 0.02, 0.68 ± 0.04 and 0.73 ± 0.03, respectively) (Figure 2A-D, M), LE marker (Rab7) (PCC, 0.72 ± 0.03) (Figure 2E), lysosome

Downloaded from http://ashpublications.org/blood/article-pdf/doi/10.1182/blood.2020007389/1799023/blood.2020007389.pdf by guest on 30 January 2021

marker (Lamp1) (PCC, 0.75 ± 0.02) (Figure 2F) and TPCN2 (likely in DG, LE or lysosome) (PCC, 0.59 ± 0.04) (Figure 2G). Consistently, live MEG-01 cells expressing Cherry-TMEM163 showed a high proportion of TMEM163 colocalization with LysoSensor Green DND-189 (PCC, 0.82 ± 0.02) (Figure 2H). [57] Therefore, TMEM163 is concentrated in acidic perinuclear DG and LE marker-positive compartments. Further analysis showed epitope-tagged TMEM163 overlapped with EE markers, EEA1 (PCC, 0.40 ± 0.02) (Figure 2I) and Rab5 (PCC, 0.63 ± 0.03) (Figure 2J). The DG positive limiting membrane protein VMAT2 overlapped to only a small proportion with EEA1 (PCC, 0.14 ± 0.01) (Supplemental Figure 3B) compared to mepacrine (PCC, 0.81 ± 0.02) (Supplemental Figure 3A). Notably, TMEM163 showed very little colocalization with AG markers (P-selectin, VWF and PF4) (PCCs, 0.13 ± 0.02, 0.04 ± 0.01 and 0.08 ± 0.01, respectively) (Figure 2K, L, Supplemental Figure 3C, D). Furthermore, sucrose density gradient centrifugation assays (Figure 2N) showed that TMEM163 fractionated in F3-F9. TMEM163 partially co-fractionated with the EE marker EEA1 in F3-F5, the LE marker Rab7 in F6-F9, and the DG marker LAMP2 in F5-F8, further indicating that TMEM163 is localized to endosomal structures. Together, these results suggest that TMEM163 localized mostly to perinuclear DG and LE marker-positive compartments (likely DG precursors) and to small vesicular structures (likely EEs) in the periphery of MEG-01 cells. The localization of TMEM163 in EE-like and DG precursor-like compartments suggests that TMEM163 may traffic from EEs to DGs.

TMEM163 interacts with BLOC-1

The decreased level of TMEM163 in BLOC-1 mouse mutants (*sdy* and *pa*, Figure 1C, D) and

Downloaded from http://ashpublications.org/blood/article-pdf/doi/10.1182/blood.2020007389/1799023/blood.2020007389.pdf by guest on 30 January 2021

an HPS-9 patient (Figure 1M) suggests that BLOC-1 may be involved in the trafficking of TMEM163. To determine whether TMEM163 is a cargo of BLOC-1, we tested for possible physical interactions between TMEM163 and the BLOC-1 subunits dysbindin, pallidin and BLOS1. Co-immunoprecipitation (Co-IP) of endogenous proteins showed that dysbindin interacted with TMEM163 (Figure 3A, B). Consistently, due to the deficiencies of dysbindin or TMEM163 in *sdy* or *Tmem163-KO* mice platelets, neither the anti-dysbindin nor the anti-TMEM163 antibody precipitated TMEM163 or dysbindin compared with their positive controls (Figure 3C, D). Furthermore, we confirmed that Flag-dysbindin-1A and Flag-BLOS1 (one of shared subunits of BLOC-1 and BORC) co-precipitated with Myc-TMEM163 by co-IP assays, but not Flag-KXD1 (one subunit of BORC) (Supplemental Figure 4A-D). Moreover, pallidin precipitated with TMEM163 in B6 mice but not in the *pa* mutant (Supplemental Figure 4E). However, the separation of dysbindin in F1-F8 suggests that dysbindin and TMEM163 do not reside in a tight complex (Figure 2N), implying that TMEM163 may be one of multiple DG proteins transported by BLOC-1. These results suggest that BLOC-1 interacts with TMEM163 during its transport from early endosomes to perinuclear DG and LE marker-positive compartments (likely DG precursors).

TMEM163 deficiency affects the biogenesis of platelet DGs

We further analyzed the morphological characteristics of *DTNBP1* and *TMEM163* deficient cell lines (*DTNBP1-KO* (*D1*, *D12* and *D24*) and *TMEM163-KO* (*T20* and *T87*) stable cell lines constructed by the CRISPR-Cas9 system as shown in Supplemental Figure 5) by thin section transmission electron microscopy (TEM). A large number of organelles were present

Downloaded from http://ashpublications.org/blood/article-pdf/doi/10.1182/blood.2020007389/1799023/blood.2020007389.pdf by guest on 30 January 2021

in WT MEG-01 cells after induction with 100 nM TPA for 4 days, including round-shaped membranous organelles resembling EEs with less intraluminal contents, LEs with more intraluminal contents and MVBs with intraluminal vesicles. Numerous enlarged round-shaped membranous organelles resembling EEs with less intraluminal contents increased significantly in *DTNBP1-KO* (*D1* and *D24*) and *TMEM163-KO* (*T20* and *T87*) MEG-01 cells (Figure 4A-C). These results suggest that deletion of dysbindin or TMEM163 resulted in the accumulation of large vacuoles.

We speculated that BLOC-1 participates in the biogenesis of DGs by regulating the transport of TMEM163 to DGs, and loss-of-function mutants of TMEM163 or BLOC-1 have similar phenotypes. To test this hypothesis, we constructed *Tmem163* knockout mice (*Tmem163-KO)* using the CRISPR-Cas9 system (Supplemental Figure 6A, B). Both the tail genomic PCR and western blotting assays proved that the *Tmem163* gene was successfully deleted (Supplemental Figure 6C-E). Through whole mount TEM experiments, which has been used as the gold standard method for diagnosing platelet DG deficiencies, [58-61] we found that DGs in *Tmem163-KO* mice were absent, which is similar to *sdy* (C57BL/6J) mice (Figure 4D, E), suggesting that TMEM163 deficiency likely affects the biogenesis of platelet DGs.

Tmem163-KO (n = 6) and C57BL/6J (B6) (n = 8) mice did not differ significantly in platelet count, mean platelet volume (MPV), and other hematological parameters (Supplemental Table 2). We observed no abnormalities in the surface expression of CD41, CD42b (GPIbα), and GPVI in *sdy* and *Tmem163-KO* platelets, compared to their controls (Supplemental Figure 7).

DGs concentrate small molecules such as serotonin, ADP, and calcium. [62,63] Consistently,

Downloaded from http://ashpublications.org/blood/article-pdf/doi/10.1182/blood.2020007389/1799023/blood.2020007389.pdf by guest on 30 January 2021

similar to *sdy* mutant, *Tmem163-KO* platelets displayed reduced ADP (Figure 4F) and serotonin (Figure 4G) relative to their littermate controls. Mepacrine, a green fluorescent dye, has a high affinity for adenine nucleotides and can be taken up by platelet DGs rapidly and selectively. Platelets of HPS patients have a significantly reduced uptake of mepacrine into DGs. [64-66] Similar to platelets of *sdy* mice, *Tmem163-KO* mouse platelets displayed significantly deficient uptake of mepacrine, relative to platelets of littermate controls, with a high dose of mepacrine (1.7 μM) (Figure 4H). In addition, we noticed that the defects in serotonin storage and mepacrine uptake were less profound in *Tmem163-KO* platelets than in *sdy* platelets, suggesting that TMEM163 plays a more specific role in DG biogenesis than BLOC-1 does.

Furthermore, we analyzed the ultrastructure of organelles in platelets of *Tmem163-KO, sdy* and *pa* (another BLOC-1 mutant [67]) mice. Based on the density of the dense core of round-shaped membranous compartments, the organelles of B6 mouse platelets were divided into two types: Type I has low electron density (the average gray value was greater than 50) and Type II has higher electron density (the average gray value was less than 50) (Supplemental Figure 8F). Statistical analysis of Type I and Type II compartments in *Tmem163-KO*, *sdy* and *pa* mutant mice, and their corresponding control mice, showed that *Tmem163-KO*, *sdy* and *pa* mutant mice displayed an abnormal Type I accumulation and decreased Type II compartments (Supplemental Figure 8A-E, G-J). We speculate that the Type I compartment represents an immature DG and the Type II compartment represents a mature DG. This requires further confirmation by future immuno-gold labeling assays.

Moreover, *Tmem163-KO* platelets displayed normal steady-state levels of AG content

Downloaded from http://ashpublications.org/blood/article-pdf/doi/10.1182/blood.2020007389/1799023/blood.2020007389.pdf by guest on 30 January 2021

and membrane proteins (basic fibroblast growth factor (bFGF), endostatin (ENDO), PF4, P-selectin, thrombospondin (TSP) and von Willebrand factor (VWF)) (Supplemental Figure 9) and showed a significantly weaker endocytosis of FGN (fibrinogen) (Supplemental Figure 10), indicating that TMEM163 deficiency does not apparently affect the biogenesis of platelet AGs. Taken together, these results demonstrate that TMEM163 deficiency affects the biogenesis of platelet DGs, but not AGs. This finding is similar to that observed in BLOC-1 deficiency.

TMEM163 deficiency impairs platelet DG secretion

We next investigated possible roles of TMEM163 in the secretion of DGs by detecting ATP release and in the secretion of AGs by measuring CD62p exposure and PF4 release. At various concentrations of collagen, *sdy* mutant and *Tmem163-KO* platelets both displayed significantly defective release of ATP compared to their littermate controls ($sdy^{+/-}$ or B6 mice) (Figure 5A, Supplemental Table 3). Consistently, at various concentrations of thrombin (0.25, 1 U/mL), *sdy* mutant and *Tmem163-KO* platelets displayed significantly defective release of ATP (Figure 5B, Supplemental Table 3). Both *sdy* and *Tmem163-KO* platelets showed impaired ATP release relative to controls in response to both collagen and thrombin. However, the defects in *Tmem163-KO* mice were milder than those in *sdy* mice, which is consistent with the milder serotonin storage and mepacrine uptake defects in the former, supporting that TMEM163 is one of multiple DG proteins transported by BLOC-1.

HPS6 deficiency displays impaired PDI secretion and impaired exocytosis of AGs, [68] and affects the tubulation and secretion of von Willebrand factor [69]. Platelets from HPS mutants pearl (*pe*), pallid (*pa*) and light ear (*le*) display impairment of AG secretion which is regarded

Downloaded from http://ashpublications.org/blood/article-pdf/doi/10.1182/blood.2020007389/1799023/blood.2020007389.pdf by guest on 30 January 2021

as secondary to deficient DG secretion. [70] Likewise, flow cytometry analysis demonstrated that *sdy* mutant and *Tmem163-KO* platelets displayed significant impairment of CD62p exposure at low doses of collagen (0.5, 1.0 μg/mL) or thrombin (0.25 U/mL) compared to their littermate controls. Notably, the defects in *Tmem163-KO* mice were relatively milder than those in *sdy* mice. Impaired AG secretion could be rescued by high doses of agonists or exogenous ADP when there is no primary AG deficiency (Figure 5C, D, Supplemental Figure 11 and 12). At higher doses of thrombin (0.5 U/mL) or with ADP supplement, CD62p levels revealed no significant differences (Figure 5C, D). Moreover, at various concentrations of collagen (0.8, 1.2, 5 μg/mL) or at low doses of thrombin (0.25 U/mL), *sdy* mutant and *Tmem163-KO* platelets displayed significantly defective PF4 release. However, a higher doses of thrombin (1 U/mL) or with ADP supplement, there was no significant difference in PF4 release (Figure 5E, F). Taken together, both *sdy* and *Tmem163-KO* platelets showed impaired AG secretion relative to controls in response to both collagen and thrombin, suggesting that the impairment of AG secretion in *sdy* and *Tmem163-KO* platelets is secondary to deficient DG secretion and that there is no *bona fide* AG defects in both mutants.

TMEM163 deficiency impairs platelet function

To determine whether the defects of DG secretion resulted in abnormal platelet aggregation, we evaluated the aggregation of washed platelets from *sdy* and *Tmem163-KO* mice stimulated with various doses of agonists in a turbidimetric aggregometer. At different doses of collagen (1.2, 2.4 μg/mL), *sdy* and *Tmem163-KO* mice showed significant impairment of platelet aggregation compared to their littermate controls (Figure 6A, B, E). Consistently, at different

Downloaded from http://ashpublications.org/blood/article-pdf/doi/10.1182/blood.2020007389/1799023/blood.2020007389.pdf by guest on 30 January 2021

doses of thrombin (0.025, 0.05 U/mL), *sdy* and *Tmem163-KO* mice showed significant impairment of platelet aggregation (Figure 6C, D, F). We further tested hemostasis in *Tmem163-KO* mice by recording tail-bleeding times. *Tmem163-KO* mice had significant prolongation in bleeding time (Figure 6G), suggesting that TMEM163 deficiency results in defective platelet aggregation and prolonged bleeding resembling the *sdy* mutant.

Tmem163-KO mice and HPS mouse mutants of BLOC-1, BLOC-2 and AP-3 show defective Zn^{2+} homeostasis

To further define the role of TMEM163 in the biogenesis of DGs, we investigated its function in megakaryocytes. TMEM163 has been shown to bind Zn^{2+} presumably as a proton-dependent Zn^{2+} transporter [45]. During blood clotting, activated platelets release a large amount of stored Zn^{2+} to the blood stream. [31,71,72] Once platelets are stimulated, the two types of secretory granules (AGs and DGs) activate. AGs store protein-bound Zn^{2+}, [73,74] but it is uncertain whether zinc ions are present in DGs. When MEG-01 cells expressing Cherry-VMAT2 were treated with zinc indicator FluoZin™-3, we found VMAT2-positive organelles enriched with FluoZin™-3 dye (Figure 7A). Furthermore, we found that TMEM163 may act as a limiting membrane protein which packages FluoZin™-3 dye (Figure 7B, C). These results suggest that perinuclear DG and LE marker-positive compartments (likely DG precursors) store free zinc.

Next, we incubated *DTNBP1-KO* and *TMEM163-KO* cell lines with FluoZin™-3 in the absence or presence of 100 μM $ZnCl_2$. We observed abnormal intracellular zinc accumulation in granule-like structures of *DTNBP1-KO* (*D1*, *D24*) and *TMEM163-KO* (*T20*, *T87*) MEG-01

Downloaded from http://ashpublications.org/blood/article-pdf/doi/10.1182/blood.2020007389/1799023/blood.2020007389.pdf by guest on 30 January 2021

cells (Supplemental Figure 13). In addition, washed platelets from *sdy* and *Tmem163-KO* mice also showed abnormal zinc accumulation compared to platelets of their littermate controls under resting conditions. Similarly, the resting platelets of other HPS mouse models of BLOC-1 (*pa*), BLOC-2 (*ru*) and AP-3 (*pe*) mice showed abnormal zinc accumulation (Figure 7D), consistent with the decreased TMEM163 expression.

Once platelets are activated by thrombin, zinc is rapidly released from granules. Our data displayed similar kinetics of decrease in platelet zinc levels in all mutant and control mice after activation by thrombin (Figure 7E-H), suggesting that zinc is mostly stored in thrombin-triggered releasable granules. However, zinc in AP-3 (*pe*) deficient mice did not decline to basal levels (Figure 7I). One explanation is that the amount of thrombin used in this assay was not sufficient to release the highly accumulated zinc in *pe* mice, as the fold change in *pe* platelets was the highest among these mutant mice (Figure 7D). Zinc accumulation in the platelets of these mutant mice may result from the defects in other Zn^{2+} transporters (ZnT/ZIP family members) residing in the organelles of platelets. However, our quantitative RT-PCR results showed normal mRNA expression of ZnT (ZNT1, 5, 6, 7 and 9) and ZIP (ZIP1, 4, 6, 7, 9 and 10) family members in mature megakaryocytes from *Tmem163-KO* mice relative to B6 mice (Supplemental Figure 14). This suggests that TMEM163 deficiency may be the major contributor of zinc accumulation in megakaryocytes and platelets.

Next, to explore whether decreasing Zn^{2+} accumulation in *sdy* and *Tmem163-KO* platelets would restore normal platelet aggregation, we incubated washed platelets with FluoZin^{TM}-3 in the presence of a Zn^{2+} chelator, TPEN, and recorded the kinetics of aggregation during resting and activated states. Both resting and activated platelets of *sdy* and

Downloaded from http://ashpublications.org/blood/article-pdf/doi/10.1182/blood.2020007389/1799023/blood.2020007389.pdf by guest on 30 January 2021

Tmem163-KO displayed reduced FluoZin^{TM}-3 intensities with the addition of TPEN (Supplemental Figure 15A-C), suggesting that TPEN effectively removes Zn^{2+} from platelets. We then incubated *sdy* and *Tmem163-KO* platelets with either 20 μM or 50 μM TPEN (DMSO as a negative control). After stimulation with 0.05 U/mL thrombin, we found that TPEN inhibited platelet aggregation in a dose dependent manner, and did not restore the impairment of platelet aggregation in *sdy* and *Tmem163-KO* mice (Supplemental Figure 15D-G), suggesting that the mutant defects occur in DG biogenesis but not in DG secretion.

Taken together, these results demonstrate that deficiency of *DTNBP1* or *TMEM163* compromises intracellular organellar Zn^{2+} homeostasis in platelets and that defective Zn^{2+} homeostasis is highly correlated with DG biogenesis.

Discussion

Using different HPS mouse models and HPS patients, we identified a previously unreported DG Zn^{2+} transporter, TMEM163, which is significantly reduced in BLOC-1 (*sdy* and *pa*), BLOC-2 (*ru*) or AP-3 (*pe*) deficient mice and HPS patients (HPS2, 3, 5, 6, or 9). Furthermore, we determined that BLOC-1 interacts with TMEM163 during its transport from early endosomes to perinuclear DG and LE marker-positive compartments (likely DG precursors). Therefore, all these mutant mice have defects in DG biogenesis and secretion, resulting in prolonged bleeding times and impaired platelet aggregation. Finally, similarly to the deficiency of BLOC-1, BLOC-2 or AP-3 which results in abnormal platelet intracellular organellar Zn^{2+} homeostasis of platelets, TMEM163 deficiency alters platelet Zn^{2+} homeostasis. These new findings are important for understanding the LRO defects in HPS and

Downloaded from http://ashpublications.org/blood/article-pdf/doi/10.1182/blood.2020007389/1799023/blood.2020007389.pdf by guest on 30 January 2021

in platelet storage pool deficiency.

From studies on melanosomes, it is reasonable to propose that HPACs are involved in platelet DG biogenesis by regulating the trafficking of multiple DG cargoes. In this study, we identified a novel membrane protein (likely a DG membrane protein), TMEM163, which interacts with BLOC-1 and is one of the multiple DG proteins transported by BLOC-1. Notably, our data demonstrated that TMEM163 was partially localized to early endosomes and was deficient in BLOC-1, BLOC-2 or AP-3 mutant mice, but was at normal levels in BLOC-3 or HOPS mutant mice. There are reports that in melanocytes and neurons, BLOC-1 and AP-3 act upstream of BLOC-2 in cargo trafficking, whereas BLOC-3 and HOPS act in different trafficking pathways. [1,2,75] Although it has been reported that RAB32 and RAB38 are required for the biogenesis of DGs, [10,16] both the expression of Rab32 and Rab38 in the platelets of *Tmem163-KO* mice showed no significant changes compared with their control mice (Supplemental Figure 16). In addition, it has been reported that BLOC-1 physically interacts with BLOC-2 or AP-3 to facilitate TYRP1 trafficking from endosomes to melanosomes. [12] Our results suggest that BLOC-1, BLOC-2 and AP-3 are functionally required for TMEM163 transport, similar to some cargoes of melanosomes [56,76] and synaptic vesicles [77,78].

Several other DG integral membrane proteins such as LAMP2, CD63 and VMAT2[10,19] have been identified, but the possible involvement of these proteins in DG biogenesis is unknown. However, the substantial combined evidence of whole mount TEM, thin section TEM and DG contents presented here strongly support the critical involvement of TMEM163 in DG biogenesis. In summary, our data are consistent with a role of HPACs in the biogenesis

Downloaded from http://ashpublications.org/blood/article-pdf/doi/10.1182/blood.2020007389/1799023/blood.2020007389.pdf by guest on 30 January 2021

of LROs, in which BLOC-1, BLOC-2 and AP-3 function in trafficking of TMEM163 from endosomes to perinuclear DG and LE marker-positive compartments (likely DG precursors). Considering that TMEM163 is specifically deficient in BLOC-1, BLOC-2 or AP-3 mouse models and HPS patients, we propose that TMEM163 or platelet zinc concentration could be a new marker for the diagnosis and genotyping of HPS subtypes.

Platelet whole mount TEM has long been the gold standard method for diagnosing platelet DG deficiencies. [58-61] As expected, *Tmem163-KO* platelets showed the typical "DG null" phenotype by this procedure. Interestingly, through thin section TEM of platelets, we found that a deficiency of TMEM163, dysbindin or pallidin causes the accumulation of the Type I compartment (likely immature DG) and decrease in the Type II compartment (likely mature DG), which requires further future confirmation by immuno-gold labeling assays. Further analysis by thin section TEM showed both *DTNBP1-KO* and *TMEM163-KO* MEG-01 cell lines have increased enlarged vacuoles, which may represent immature DGs or DG precursors in megakaryocytes. However, the underlying mechanisms of DG maturation during megakaryocyte differentiation require further investigation.

A previous report demonstrated that TMEM163 lies within the limiting membrane of synaptic vesicles (SVs). [41] Both SVs and DGs belong to LROs. [2] It has been reported that TRPML1 interacts with TMEM163 to regulate the trafficking of TMEM163 from the plasma membrane to endocytic compartments, lysosomes or SVs. TMEM163 was proposed as a zinc (Zn^{2+})/proton (H^+) exchanger and as a cooperative ionic channel with TRPML1 in lysosomes. TMEM163 functions in influxing zinc into the cytoplasm from the extracellular matrix and from the lumen of vesicular compartments, [43,44] indicating that TMEM163 acts as a ZIP

Downloaded from http://ashpublications.org/blood/article-pdf/doi/10.1182/blood.2020007389/1799023/blood.2020007389.pdf by guest on 30 January 2021

protein not a ZNT protein. However, another study reported that TMEM163 effluxes zinc from the cytosol. Thus, TMEM163 was designated as ZNT11, a new member of the ZNT family. [48] When SV31 is reconstituted in liposomes, TMEM163 assembles into a dimer and functions as a proton-dependent Zn^{2+} transporter, similar to ZNT3. [45] Our investigation indicated that deficiency of TMEM163 results in abnormal intracellular zinc content (accumulation in granule-like structures), thus affecting the biogenesis and function of DGs. We speculate that TMEM163 acts as a ZIP protein on DGs as zinc is accumulated in granule-like structures when TMEM163 is deficient (Figure 7). Accumulated Zn^{2+} in platelets with a TMEM163 deficiency (or BLOC-1, BLOC-2 or AP-3 deficiency) may disrupt the ion homeostasis that is essential for DG biogenesis and secretion.

Downloaded from http://ashpublications.org/blood/article-pdf/doi/10.1182/blood.2020007389/1799023/blood.2020007389.pdf by guest on 30 January 2021

Acknowledgements

We are very thankful to Dr. Richard T. Swank who provided the mutant mice in this study and proofread this manuscript. We are very thankful to Dr. Runlin Z. Ma who provided the pSpCas9 (BB)-2A-GFP (PX458) vector, Dr. Fangyuan Nie who helped to analyze qRT-PCR data and Dr. Chang Zhang who provided the pEGFP-C2-Rab5, pEGFP-C2-Rab7 and pEGFP-C2-Lamp1 vectors. We are very thankful to Dr. Jiaying Yu, Ms. Jiran Lu and Mr. Huipeng Wang for the help in breeding several mutant mice. This work was supported by grants from the Ministry of Science and Technology of China (2019YFA0802104) and from National Natural Science Foundation of China (31800977; 91954000; 31830054; 91539204; 31900496).

Authorship Contributions

Y.Y. and W.L. designed the research, analyzed the data and wrote the manuscript. Y.Y. performed most of the experiments; T.Liu and A.W. recruited all the subjects and collected the written informed consents; Y.C. participated in *Tmem163-KO* mouse generation; W.Z. and Q.C. assisted in the design of platelet aggregation assays; T.Li provided technical support for flow cytometry; L.Y. provided technical support for electron microscopy; X.H. and Y.W. helped to analyze mass spectrometry data.

Disclosure of Conflicts of Interest

The authors declare no competing financial interests.

Data sharing: For original data, please contact the corresponding author.

References

1. Huizing M, Anikster Y, Gahl WA. Hermansky-Pudlak syndrome and related disorders of organelle formation. Traffic. 2000;1(11):823-835.
2. Wei AH, Li W. Hermansky-Pudlak syndrome: pigmentary and non-pigmentary defects and their pathogenesis. Pigment Cell Melanoma Res. 2013;26(2):176-192.
3. Dell'Angelica EC, Mullins C, Caplan S, Bonifacino JS. Lysosome-related organelles. FASEB J. 2000;14(10):1265-1278.
4. Huizing M, Helip-Wooley A, Westbroek W, Gunay-Aygun M, Gahl WA. Disorders of lysosome-related organelle biogenesis: clinical and molecular genetics. Annu Rev Genomics Hum Genet. 2008;9:359-386.
5. Swank RT, Novak EK, McGarry MP, Rusiniak ME, Feng L. Mouse models of Hermansky Pudlak syndrome: a review. Pigment Cell Res. 1998;11(2):60-80.
6. Wei ML. Hermansky-Pudlak syndrome: a disease of protein trafficking and organelle function. Pigment Cell Res. 2006;19(1):19-42.
7. Raposo G, Marks MS, Cutler DF. Lysosome-related organelles: driving post-Golgi compartments into specialisation. Curr Opin Cell Biol. 2007;19(4):394-401.
8. Ambrosio AL, Di Pietro SM. Storage pool diseases illuminate platelet dense granule biogenesis. Platelets. 2017;28(2):138-146.

Downloaded from http://ashpublications.org/blood/article-pdf/doi/10.1182/blood.2020007389/1799023/blood.2020007389.pdf by guest on 30 January 2021

9. Chen Y, Yuan Y, Li W. Sorting machineries: how platelet-dense granules differ from alpha-granules. Biosci Rep. 2018;38(5) : BSR20180458.
10. Ambrosio AL, Boyle JA, Di Pietro SM. Mechanism of platelet dense granule biogenesis: study of cargo transport and function of Rab32 and Rab38 in a model system. Blood. 2012;120(19):4072-4081.
11. Peden AA, Oorschot V, Hesser BA, Austin CD, Scheller RH, Klumperman J. Localization of the AP-3 adaptor complex defines a novel endosomal exit site for lysosomal membrane proteins. J Cell Biol. 2004;164(7):1065-1076.
12. Di Pietro SM, Falcon-Perez JM, Tenza D, et al. BLOC-1 interacts with BLOC-2 and the AP-3 complex to facilitate protein trafficking on endosomes. Mol Biol Cell. 2006;17(9):4027-4038.
13. Reddington M, Novak EK, Hurley E, Medda C, McGarry MP, Swank RT. Immature dense granules in platelets from mice with platelet storage pool disease. Blood. 1987;69(5):1300-1306.
14. Youssefian T, Cramer EM. Megakaryocyte dense granule components are sorted in multivesicular bodies. Blood. 2000;95(12):4004-4007.
15. Hanby HA, Bao J, Noh JY, et al. Platelet dense granules begin to selectively accumulate mepacrine during proplatelet formation. Blood Adv. 2017;1(19):1478-1490.
16. Aguilar A, Weber J, Boscher J, et al. Combined deficiency of RAB32 and RAB38 in the mouse mimics Hermansky-Pudlak syndrome and critically impairs thrombosis. Blood Adv. 2019;3(15):2368-2380.
17. Meng R, Wang Y, Yao Y, et al. SLC35D3 delivery from megakaryocyte early endosomes is required for platelet dense granule biogenesis and is differentially defective in Hermansky-Pudlak syndrome models. Blood. 2012;120(2):404-414.
18. Chintala S, Tan J, Gautam R, et al. The Slc35d3 gene, encoding an orphan nucleotide sugar transporter, regulates platelet-dense granules. Blood. 2007;109(4):1533-1540.
19. Ambrosio AL, Boyle JA, Di Pietro SM. TPC2 mediates new mechanisms of platelet dense granule membrane dynamics through regulation of Ca2+ release. Mol Biol Cell. 2015;26(18):3263-3274.
20. Ambrosio AL, Boyle JA, Aradi AE, Christian KA, Di Pietro SM. TPC2 controls pigmentation by regulating melanosome pH and size. Proc Natl Acad Sci U S A. 2016;113(20):5622-5627.
21. Zhang Z, Gong J, Sviderskaya EV, Wei A, Li W. Mitochondrial NCKX5 regulates melanosomal biogenesis and pigment production. J Cell Sci. 2019;132(14) :jcs232009.
22. Apgar J. Effect of zinc deficiency on parturition in the rat. Am J Physiol. 1968;215(1):160-163.
23. Emery MP, Browning JD, O'Dell BL. Impaired hemostasis and platelet function in rats fed low zinc diets based on egg white protein. J Nutr. 1990;120(9):1062-1067.
24. O'Dell BL, Reynolds G, Reeves PG. Analogous effects of zinc deficiency and aspirin toxicity in the pregnant rat. J Nutr. 1977;107(7):1222-1228.
25. Stefanini M. Cutaneous bleeding related to zinc deficiency in two cases of advanced cancer. Cancer. 1999;86(5):866-870.
26. Gordon PR, Browning JD, O'Dell BL. Platelet arachidonate metabolism and platelet function in zinc-deficient rats. J Nutr. 1983;113(4):766-772.

Downloaded from http://ashpublications.org/blood/article-pdf/doi/10.1182/blood.2020007389/1799023/blood.2020007389.pdf by guest on 30 January 2021

27. Gordon PR, O'Dell BL. Rat platelet aggregation impaired by short-term zinc deficiency. J Nutr. 1980;110(10):2125-2129.
28. Gordon PR, Woodruff CW, Anderson HL, O'Dell BL. Effect of acute zinc deprivation on plasma zinc and platelet aggregation in adult males. Am J Clin Nutr. 1982;35(1):113-119.
29. Marx G, Krugliak J, Shaklai M. Nutritional zinc increases platelet reactivity. Am J Hematol. 1991;38(3):161-165.
30. Taylor KA, Pugh N. The contribution of zinc to platelet behaviour during haemostasis and thrombosis. Metallomics. 2016;8(2):144-155.
31. Watson BR, White NA, Taylor KA, et al. Zinc is a transmembrane agonist that induces platelet activation in a tyrosine phosphorylation-dependent manner. Metallomics. 2016;8(1):91-100.
32. Baltaci AK, Yuce K. Zinc Transporter Proteins. Neurochem Res. 2018;43(3):517-530.
33. Costas J. Comment on "current understanding of ZIP and ZnT zinc transporters in human health and diseases". Cell Mol Life Sci. 2015;72(1):197-198.
34. Eide DJ. Zinc transporters and the cellular trafficking of zinc. Biochim Biophys Acta. 2006;1763(7):711-722.
35. Huang L, Tepaamorndech S. The SLC30 family of zinc transporters - a review of current understanding of their biological and pathophysiological roles. Mol Aspects Med. 2013;34(2-3):548-560.
36. Jeong J, Eide DJ. The SLC39 family of zinc transporters. Mol Aspects Med. 2013;34(2-3):612-619.
37. Kambe T, Hashimoto A, Fujimoto S. Current understanding of ZIP and ZnT zinc transporters in human health and diseases. Cell Mol Life Sci. 2014;71(17):3281-3295.
38. Schweigel-Rontgen M. The families of zinc (SLC30 and SLC39) and copper (SLC31) transporters. Curr Top Membr. 2014;73:321-355.
39. Kambe T, Tsuji T, Hashimoto A, Itsumura N. The Physiological, Biochemical, and Molecular Roles of Zinc Transporters in Zinc Homeostasis and Metabolism. Physiol Rev. 2015;95(3):749-784.
40. Yamasaki S, Sakata-Sogawa K, Hasegawa A, et al. Zinc is a novel intracellular second messenger. J Cell Biol. 2007;177(4):637-645.
41. Burre J, Zimmermann H, Volknandt W. Identification and characterization of SV31, a novel synaptic vesicle membrane protein and potential transporter. J Neurochem. 2007;103(1):276-287.
42. Barth J, Zimmermann H, Volknandt W. SV31 is a Zn2+-binding synaptic vesicle protein. J Neurochem. 2011;118(4):558-570.
43. Cuajungco MP, Basilio LC, Silva J, et al. Cellular zinc levels are modulated by TRPML1-TMEM163 interaction. Traffic. 2014;15(11):1247-1265.
44. Cuajungco MP, Kiselyov K. The mucolipin-1 (TRPML1) ion channel, transmembrane-163 (TMEM163) protein, and lysosomal zinc handling. Front Biosci (Landmark Ed). 2017;22:1330-1343.
45. Waberer L, Henrich E, Peetz O, et al. The synaptic vesicle protein SV31 assembles into a dimer and transports Zn(2). J Neurochem. 2017;140(2):280-293.
46. Eichelsdoerfer JL, Evans JA, Slaugenhaupt SA, Cuajungco MP. Zinc dyshomeostasis is linked with the loss of mucolipidosis IV-associated TRPML1 ion channel. J Biol Chem.

Downloaded from http://ashpublications.org/blood/article-pdf/doi/10.1182/blood.2020007389/1799023/blood.2020007389.pdf by guest on 30 January 2021

2010;285(45):34304-34308.
47. Chakraborty S, Vellarikkal SK, Sivasubbu S, Roy SS, Tandon N, Bharadwaj D. Role of Tmem163 in zinc-regulated insulin storage of MIN6 cells: Functional exploration of an Indian type 2 diabetes GWAS associated gene. Biochemical and Biophysical Research Communications. 2020;522(4):1022-1029.
48. Sanchez VB, Ali S, Escobar A, Cuajungco MP. Transmembrane 163 (TMEM163) protein effluxes zinc. Arch Biochem Biophys. 2019;677:108166.
49. Li W, Zhang Q, Oiso N, et al. Hermansky-Pudlak syndrome type 7 (HPS-7) results from mutant dysbindin, a member of the biogenesis of lysosome-related organelles complex 1 (BLOC-1). Nat Genet. 2003;35(1):84-89.
50. Li W, Rusiniak ME, Chintala S, Gautam R, Novak EK, Swank RT. Murine Hermansky-Pudlak syndrome genes: regulators of lysosome-related organelles. Bioessays. 2004;26(6):616-628.
51. Liu T, Yuan Y, Bai D, et al. Genetic variants and mutational spectrum of Chinese Hermansky-Pudlak syndrome patients. Pigment Cell Melanoma Res. 2020;doi: 10.1111/pcmr.12916.
52. Bultema JJ, Ambrosio AL, Burek CL, Di Pietro SM. BLOC-2, AP-3, and AP-1 proteins function in concert with Rab38 and Rab32 proteins to mediate protein trafficking to lysosome-related organelles. J Biol Chem. 2012;287(23):19550-19563.
53. Gerondopoulos A, Langemeyer L, Liang JR, Linford A, Barr FA. BLOC-3 mutated in Hermansky-Pudlak syndrome is a Rab32/38 guanine nucleotide exchange factor. Curr Biol. 2012;22(22):2135-2139.
54. Kloer DP, Rojas R, Ivan V, et al. Assembly of the biogenesis of lysosome-related organelles complex-3 (BLOC-3) and its interaction with Rab9. J Biol Chem. 2010;285(10):7794-7804.
55. Ohishi Y, Kinoshita R, Marubashi S, Ishida M, Fukuda M. The BLOC-3 subunit HPS4 is required for activation of Rab32/38 GTPases in melanogenesis, but its Rab9 activity is dispensable for melanogenesis. J Biol Chem. 2019;294(17):6912-6922.
56. Dennis MK, Delevoye C, Acosta-Ruiz A, et al. BLOC-1 and BLOC-3 regulate VAMP7 cycling to and from melanosomes via distinct tubular transport carriers. J Cell Biol. 2016;214(3):293-308.
57. Lin HJ, Herman P, Kang JS, Lakowicz JR. Fluorescence lifetime characterization of novel low-pH probes. Anal Biochem. 2001;294(2):118-125.
58. Yang Q, He X, Yang L, et al. The BLOS1-interacting protein KXD1 is involved in the biogenesis of lysosome-related organelles. Traffic. 2012;13(8):1160-1169.
59. Wei A, Yuan Y, Bai D, et al. NGS-based 100-gene panel of hypopigmentation identifies mutations in Chinese Hermansky-Pudlak syndrome patients. Pigment Cell Melanoma Res. 2016;29(6):702-706.
60. Wei A, Yuan Y, Qi Z, et al. Instability of BLOC-2 and BLOC-3 in Chinese patients with Hermansky-Pudlak syndrome. Pigment Cell Melanoma Res. 2019;32(3):373-380.
61. White JG. The dense bodies of human platelets: inherent electron opacity of the serotonin storage particles. Blood. 1969;33(4):598-606.
62. Caranobe C, Sie P, Boneu B. Serotonin uptake and storage in human platelet density subpopulations. Br J Haematol. 1982;52(2):253-258.

Downloaded from http://ashpublications.org/blood/article-pdf/doi/10.1182/blood.2020007389/1799023/blood.2020007389.pdf by guest on 30 January 2021

63. McNicol A, Israels SJ. Platelet dense granules: structure, function and implications for haemostasis. Thromb Res. 1999;95(1):1-18.
64. Gordon N, Thom J, Cole C, Baker R. Rapid detection of hereditary and acquired platelet storage pool deficiency by flow cytometry. Br J Haematol. 1995;89(1):117-123.
65. Ramstrom AS, Fagerberg IH, Lindahl TL. A flow cytometric assay for the study of dense granule storage and release in human platelets. Platelets. 1999;10(2-3):153-158.
66. Wall JE, Buijs-Wilts M, Arnold JT, et al. A flow cytometric assay using mepacrine for study of uptake and release of platelet dense granule contents. Br J Haematol. 1995;89(2):380-385.
67. Huang L, Kuo YM, Gitschier J. The pallid gene encodes a novel, syntaxin 13-interacting protein involved in platelet storage pool deficiency. Nat Genet. 1999;23(3):329-332.
68. Sharda A, Kim SH, Jasuja R, et al. Defective PDI release from platelets and endothelial cells impairs thrombus formation in Hermansky-Pudlak syndrome. Blood. 2015;125(10):1633-1642.
69. Ma J, Zhang Z, Yang L, Kriston-Vizi J, Cutler DF, Li W. BLOC-2 subunit HPS6 deficiency affects the tubulation and secretion of von Willebrand factor from mouse endothelial cells. J Genet Genomics. 2016;43(12):686-693.
70. Meng R, Wu J, Harper DC, et al. Defective release of alpha granule and lysosome contents from platelets in mouse Hermansky-Pudlak syndrome models. Blood. 2015;125(10):1623-1632.
71. Mahdi F, Madar ZS, Figueroa CD, Schmaier AH. Factor XII interacts with the multiprotein assembly of urokinase plasminogen activator receptor, gC1qR, and cytokeratin 1 on endothelial cell membranes. Blood. 2002;99(10):3585-3596.
72. Stadler N, Stanley N, Heeneman S, et al. Accumulation of zinc in human atherosclerotic lesions correlates with calcium levels but does not protect against protein oxidation. Arterioscler Thromb Vasc Biol. 2008;28(5):1024-1030.
73. Gorodetsky R, Mou X, Blankenfeld A, Marx G. Platelet multielemental composition, lability, and subcellular localization. Am J Hematol. 1993;42(3):278-283.
74. Kiran Gotru S, van Geffen JP, Nagy M, et al. Defective Zn(2+) homeostasis in mouse and human platelets with alpha- and delta-storage pool diseases. Sci Rep. 2019;9(1):8333.
75. Luzio JP, Hackmann Y, Dieckmann NM, Griffiths GM. The biogenesis of lysosomes and lysosome-related organelles. Cold Spring Harb Perspect Biol. 2014;6(9):a016840.
76. Sitaram A, Dennis MK, Chaudhuri R, et al. Differential recognition of a dileucine-based sorting signal by AP-1 and AP-3 reveals a requirement for both BLOC-1 and AP-3 in delivery of OCA2 to melanosomes. Mol Biol Cell. 2012;23(16):3178-3192.
77. Newell-Litwa K, Salazar G, Smith Y, Faundez V. Roles of BLOC-1 and adaptor protein-3 complexes in cargo sorting to synaptic vesicles. Mol Biol Cell. 2009;20(5):1441-1453.
78. Salazar G, Craige B, Styers ML, et al. BLOC-1 complex deficiency alters the targeting of adaptor protein complex-3 cargoes. Mol Biol Cell. 2006;17(9):4014-4026.

Downloaded from http://ashpublications.org/blood/article-pdf/doi/10.1182/blood.2020007389/1799023/blood.2020007389.pdf by guest on 30 January 2021

Figure Legends

Figure 1. TMEM163 is reduced in platelets from HPS mouse models and patients of BLOC-1, BLOC-2 and AP-3, but not of BLOC-3. (**A, B**) Quantitative protein identification using liquid chromatograph-mass spectrometer (LC-MS) of whole platelet lysates in *sdy* mice compared with *sdy*$^{+/-}$ mice (ctrl). 195 proteins (listed in Supplemental Table 1) were selected using the student's *t* test and quantified with high confidence ($P < 0.05$). Hierarchy clustering of the z-scored isobaric tag for relative and absolute quantitation (iTRAQ) ratio of *sdy* to *sdy*$^{+/-}$ was used to evaluate the reproducibility of the experiments (A). The expression of TMEM163 in the platelets of *sdy* mice showed significant reduction compared to *sdy*$^{+/-}$ mice (B). n = 3, * $P < 0.05$. (**C-J**) Immunoblotting analysis of TMEM163 in platelets isolated from control mice and congenic HPS mutant mouse platelets with antibodies to TMEM163 or to actin (a loading control). The expression of TMEM163 in platelets of *sdy* (BLOC-1-deficient HPS7 mutant), *pa* (BLOC-1-deficient HPS9 mutant), *ru* (BLOC-2-deficient HPS6 mutant), *pe* (AP-3-deficient HPS2 mutant) and *ru/ep* (BLOC-3-deficient model) double mutant mice (both BLOC-2 and BLOC-3-deficient model) are significantly reduced compared with control mice (C-F, I). The expression of TMEM163 in platelets of *ep*, *bf* (the VPS33A^{D251E} mutation model) and *bf/ep* showed no significant change compared with control mice (G, H, J). (**K**) TMEM163 band intensities were measured from at least 4 pairs of mice, normalized to actin levels, and expressed as the percentage (mean ± SEM) of the mean normalized value for control mice. *$P < 0.05$; **$P < 0.01$; ***$P < 0.001$; N.S., not significant. (**L**) Immunoblotting assays showed the reduced TMEM163 in BLOC-2 deficient patients (2 HPS3, 2 HPS5, 3 HPS6) compared with the healthy control (father or mother of each patient). (**M**) Immunoblotting assays showed normal TMEM163 in BLOC-3 deficient patients (3 HPS1, 1 HPS4) and reduced TMEM163 in AP-3 deficient patient (1 HPS2) and BLOC-1 deficient patient (1 HPS9) compared with the healthy control (father or mother of each patient). (**N**) Quantitative analysis of the TMEM163 band intensities. Each bar represents the percentage (mean ± SEM) of the mean normalized value for healthy control from three independent experiments. *$P < 0.05$; **$P < 0.01$; ***$P < 0.001$; N.S., not significant.

Downloaded from http://ashpublications.org/blood/article-pdf/doi/10.1182/blood.2020007389/1799023/blood.2020007389.pdf by guest on 30 January 2021

Figure 2. TMEM163 is localized to perinuclear DG and LE marker-positive compartments (likely DG precursors) and small vesicular structures (likely EEs) in the periphery, but not to AGs in MEG-01 cells. (**A-B**) MEG-01 cells were co-transfected with TMEM163-GFP or Cherry-TMEM163 and Cherry-VMAT2 (A) or GFP-VMAT2 (B) for 48 h, respectively. (**C**) MEG-01 cells were transfected with Cherry-TMEM163 for 48 h, then treated with 50 uM mepacrine for 30 minutes at 37°C. (**D**) MEG-01 cells were transfected with TMEM163-GFP for 48 h, then fixed and stained with antibodies against CD63. (**E-F**) MEG-01 cells were co-transfected with Cherry-TMEM163 and GFP-Rab7 (E) or GFP-Lamp1 (F) for 48 h, respectively. (**G**) MEG-01 cells were co-transfected with GFP-TMEM163 and Cherry-TPCN2 for 48 h, respectively. (**H**) MEG-01 cells were transfected with Cherry-TMEM163 for 48 h and treated with LysoSensor Green DND-189 for 30 minutes at 37°C. (**I**) MEG-01 cells were transfected with TMEM163-GFP for 48 h, then fixed and stained with antibodies against EEA1. (**J**) MEG-01 cells were co-transfected with Cherry-TMEM163 and GFP-Rab5 for 48 h. (**K-L**) MEG-01 cells were transfected with GFP-TMEM163 for 48 h, then fixed and stained with antibodies against P-selectin (K) or VWF (L). Pictures shown in (A-L) are representative confocal images. Outlines of cells are indicated by white lines. Insets show 5× magnified images of the boxed region. Scale bar: 10 μm. (**M**) Colocalization analysis of results shown in A-L; Pearson's correlation coefficient, 0.74 ± 0.04, 0.76 ± 0.02, 0.68 ± 0.04, 0.73 ± 0.03, 0.72 ± 0.03, 0.75 ± 0.02, 0.59 ± 0.04, 0.82 ± 0.02, 0.40 ± 0.02, 0.63 ± 0.03, 0.13 ± 0.02, 0.04 ± 0.01; n=11, 14, 8, 17, 7, 14, 13, 15, 22, 19, 10 and 10 cells, respectively. Pearson's correlation coefficient ≥ 0.4 (dotted line) represents colocalization. (**N**) Sucrose (10%-60%) gradient assay shows that TMEM163 coexists with the early endosome marker EEA1, late endosome marker Rab7 and DG marker LAMP2.

Figure 3. TMEM163 interacts with dysbindin. (**A**) Co-IP of endogenous platelet proteins show that dysbindin precipitates TMEM163. (**B**) Co-IP of endogenous platelet proteins show that TMEM163 precipitated dysbindin. The IgG was used as a negative control. (**C**) Co-IP of endogenous platelet proteins show that dysbindin precipitated TMEM163 in *sdy*$^{+/-}$ platelets

Downloaded from http://ashpublications.org/blood/article-pdf/doi/10.1182/blood.2020007389/1799023/blood.2020007389.pdf by guest on 30 January 2021

but not in *sdy* platelets. (**D**) Co-IP of endogenous platelet proteins show that TMEM163 precipitated dysbindin in wild-type (B6, C57BL/6J) platelets but not in *Tmem163-KO* platelets. All the inputs corresponded to 8 % of whole platelet lysates.

Figure 4. Ultrastructures of DGs in MEG-01 cells and platelets with deficiencies in dysbindin or TMEM163. (**A**) Thin section TEM pictures of *DTNBP1-KO* (*D1* and *D24*) and *TMEM163-KO* (*T20* and *T87*) MEG-01 cells after induction with 100 nM TPA for 4 days. The red arrows represent round-shaped membranous organelles resembling early endosomes with reduced intraluminal contents, the yellow arrows represent round-shaped membranous organelles resembling late endosomes with increased intraluminal contents, and the blue arrows represent MVB circular membranous organelles. Scale bar = 1 μm. (**B**) The average number of vacuolar compartment (the red arrows represent which shown in A) per unit area (μm^2) in *DTNBP1-KO* (*D1* and *D24*) and *TMEM163-KO* (*T20* and *T87*) MEG-01 cells are significantly higher than that in control (WT) cells (WT, 0.027 ± 0.002, n=47; *D1*, 0.037 ± 0.003, n=48; *D24*, 0.036 ± 0.002, n=52; *T20*, 0.042 ± 0.003, n=55; *T87*, 0.044 ± 0.004, n=40). (**C**) The average size of vacuolar compartment (μm^2) in *DTNBP1-KO* (*D1* and *D24*) and *TMEM163-KO* (*T20* and *T87*) MEG-01 cells are significantly larger than that in WT cells (WT, 1.343 ± 0.080, n=158; *D1*, 3.637 ± 0.234, n=299; *D24*, 3.736 ± 0.302, n=273; *T20*, 2.791 ± 0.145, n=382; *T87*, 3.890 ± 0.245, n=304). (**D, E**) TEM pictures of whole-mount platelets of the B6 (wild-type, C57BL/6J), *sdy* mutant and *Tmem163-KO* mice. Arrows show the platelet DGs. Lighter intensity dots or smaller dots (diameter less than 100 nm) are not counted as DGs. Scale bar = 0.5 μm. DGs are absent in *sdy* (0.029 ± 0.020, n=69) and *Tmem163-KO* (0.095 ± 0.020, n=222) mice compared with B6 (7.069 ± 0.451, n=58). (**F, G**) Washed platelets were lysed by 100 μL ice-cold lysis buffer, and the lysates for further ELISA assay were analyzed spectrophotometrically at 450nm. The content of platelet ADP (*sdy* vs *Tmem163-KO*, 75.71% vs. 79.77%, n = 4, 13, respectively) (F) and serotonin (*sdy* vs. *Tmem163-KO*, 33.01% vs 79.51%, n = 6, 10, respectively) (G) of *sdy, Tmem163-KO* were calculated and plotted relative to their control littermates ($sdy^{+/-}$ or B6). (**H**) Platelets were incubated with 1.7 μM mepacrine at 37°C for 30 minutes, and then analyzed by flow cytometry. The mepacrine uptake (green) fluorescence of *sdy* and *Tmem163-KO* was

Downloaded from http://ashpublications.org/blood/article-pdf/doi/10.1182/blood.2020007389/1799023/blood.2020007389.pdf by guest on 30 January 2021

expressed as the percentage (mean ± SEM) of the mean normalized value for control mice (*sdy* vs *Tmeme163-KO*, 85.41% vs. 89.29%, n = 9, 8, respectively). $*P < 0.05$; $**P < 0.01$; $***P < 0.001$.

Figure 5. *Sdy* and *Tmem163-KO* platelets display significant impairment of DG release and AG secretion. (**A, B**) Washed platelets from $sdy^{+/-}$, *sdy*, B6 (wild-type, C57BL/6J) or *Tmem163-KO* mice were stimulated with various concentrations of collagen (1.2, 5, 20 μg/mL) (A) or thrombin (0.25, 1 U/mL) (B) and secretion of ATP assessed by ATP determination kit. Data shown represent the relative ATP release as the percentage (mean ± SEM) of the mean normalized value in maximal dose stimulation for their control mice. (**C, D**) Washed platelets from $sdy^{+/-}$, *sdy*, B6 or *Tmem163-KO* mice were labeled with FITC-CD62p antibody and stimulated with various concentrations of collagen (0.5, 1.0 μg/mL, *sdy* vs *Tmem163-KO*, n = 6, 6, respectively) (C) or thrombin (0.25, 0.5U/mL, *sdy* vs *Tmem163-KO*, n = 3, 6, respectively) (D) for 5 minutes in the absence or presence of 10 μM ADP, and then measured by flow cytometry for CD62p surface expression. Data shown represent the percentage of platelets with labeling above the background level observed on unstimulated platelets. (**E, F**) Washed platelets from $sdy^{+/-}$, *sdy*, B6 or *Tmem163-KO* mice were stimulated with various concentrations of collagen (0.8, 1.2, 5.0 μg/mL) (E) or thrombin (0, 0.25, 1 U/mL) (F) for 5 minutes in the absence or presence of 10 μM ADP, and then supernatants were collected and measured by ELISA for PF-4 (*sdy* vs *Tmem163-KO*, n = 4, 4, respectively.). Data shown represent the relative PF4 release as the percentage (mean ± SEM) of the mean normalized value in maximal dose stimulation for their control mice. $*P < 0.05$; $**P < 0.01$; $***P < 0.001$; N.S., not significant.

Figure 6. *Sdy* and *Tmem163-KO* display significant impairment of platelet aggregation and prolonged bleeding time. (**A-F**) Washed platelets from $sdy^{+/-}$, *sdy*, B6 (wild-type, C57BL/6J) or *Tmem163-KO* mice were stimulated with various concentrations of collagen ($sdy^{+/-}$ vs *sdy*, 39.38% vs 11.04% (1.2 μg/mL), 71.05% vs 9.71% (2.4 μg/mL), n = 4, 4, 3, 3, respectively; B6 vs *Tmem163-KO*, 51.50% vs 13.80% (1.2 μg/mL), 80.42% vs 33.65% (2.4 μg/mL), n = 4, 4, 4, 4, respectively.) (A, B, E) or thrombin ($sdy^{+/-}$ vs *sdy*, 31.91% vs 6.53%

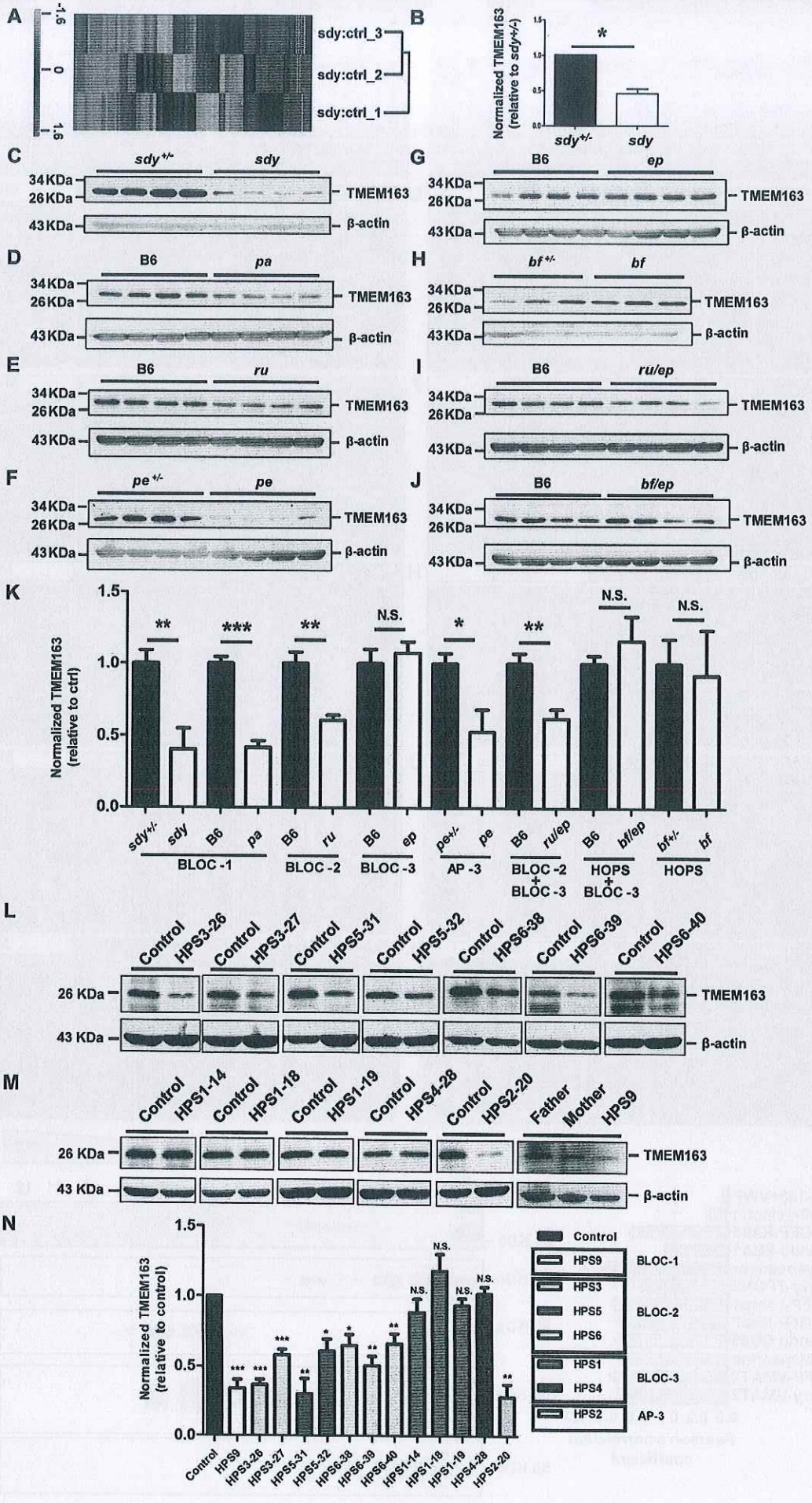
Downloaded from http://ashpublications.org/blood/article-pdf/doi/10.1182/blood.2020007389/1799023/blood.2020007389.pdf by guest on 30 January 2021

(0.025 U/mL), 68.03% vs 27.78% (0.05 U/mL), n = 4, 5, 3, 3, respectively; B6 vs *Tmem163-KO*, 21.60% vs 0.99% (0.025 U/mL), 65.01% vs 25.44% (0.05 U/mL), n = 9, 7, 7, 6, respectively.) (C, D, F) and aggregation assessed by a turbidimetric aggregometer. (**G**) Tail bleeding assays showed *Tmem163-KO* mice have prolonged bleeding times compared with B6 mice (B6, 135 ± 27.59 s; n = 9; *Tmem163-KO*, > 900 s; n = 12). Student's *t*-test, $*P < 0.05$; $**P < 0.01$; $***P < 0.001$.

Figure 7. Defective Zn^{2+} homeostasis in platelets from *Tmem163-KO* mice and HPS mouse models of BLOC-1, BLOC-2 and AP-3. (**A-B**) MEG-01 cells were transfected with Cherry-VMAT2 (A) or Cherry-TMEM163 (B) for 48 h, then incubated with 2 μM zinc indicator FluoZin™-3 for 30 minutes at 37°C. Pictures are representative confocal images. Outline of cell is indicated by the white line. Insets show 5× magnified images of the boxed region. Scale bar: 10 μm. (**C**) MEG-01 cells were transfected with Cherry-TMEM163 for 48 h, then incubated with 2 μM zinc indicator FluoZin™-3 for 30 minutes at 37°C. Picture (left) is representative Maximum Intensity Projection (MIP) image in X-Y, X-Z and Y-Z planes. Pictures (right) are Z-stack images in different dimensions. The arrows represent the classical colocalization of Cherrry-TMEM163 with FluoZin™-3. (**D-I**) Washed mutant and control mice platelets were incubated with 2.5 μM FluoZin™-3 and stimulated with 0.01 U/mL thrombin, and kinetic curve of fluorescence changes was recorded by flow cytometry (appending the first 50 seconds (Resting stage) to 400 seconds (Activated stage)). Data shown are the quantitative results (D) of normalized FluoZin3-MFI relative to each control mice at resting condition and representative kinetic curves of zinc release after thrombin treatment (E-I). B6 vs *Tmem163-KO*, n=11, 11, $sdy^{+/-}$ vs *sdy*, n=10, 10, $pa^{+/-}$ vs *pa*, n=12, 12, $ru^{+/-}$ vs *ru*, n=12, 12, $pe^{+/-}$ vs *pe*, n=12, 12, respectively. MFI: mean fluorescence intensities. Mean ± SEM, $**P < 0.01$; $***P < 0.001$; N.S., not significant.

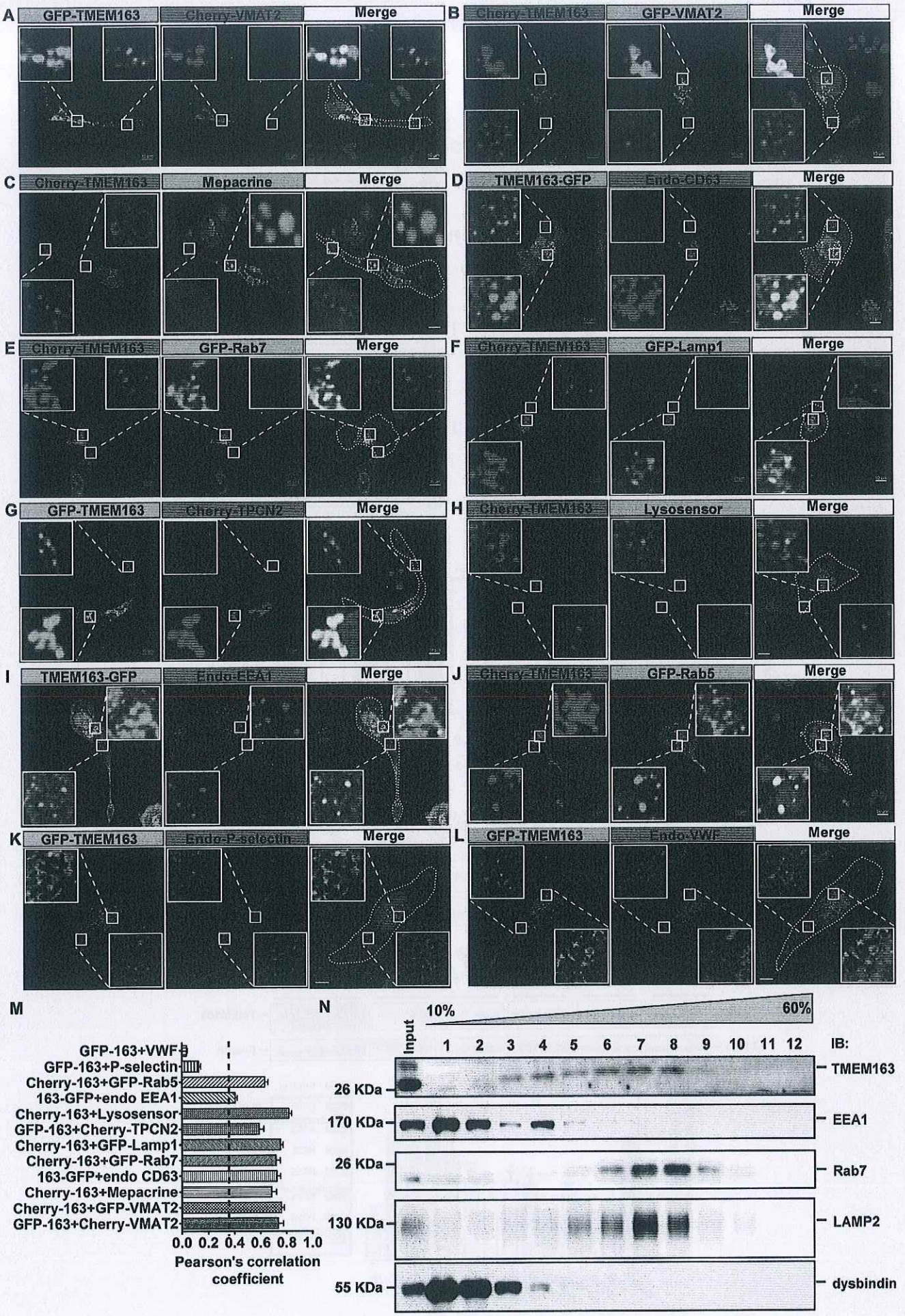
Downloaded from http://ashpublications.org/blood/article-pdf/doi/10.1182/blood.2020007389/1799023/blood.2020007389.pdf by guest on 30 January 2021

Figure 1



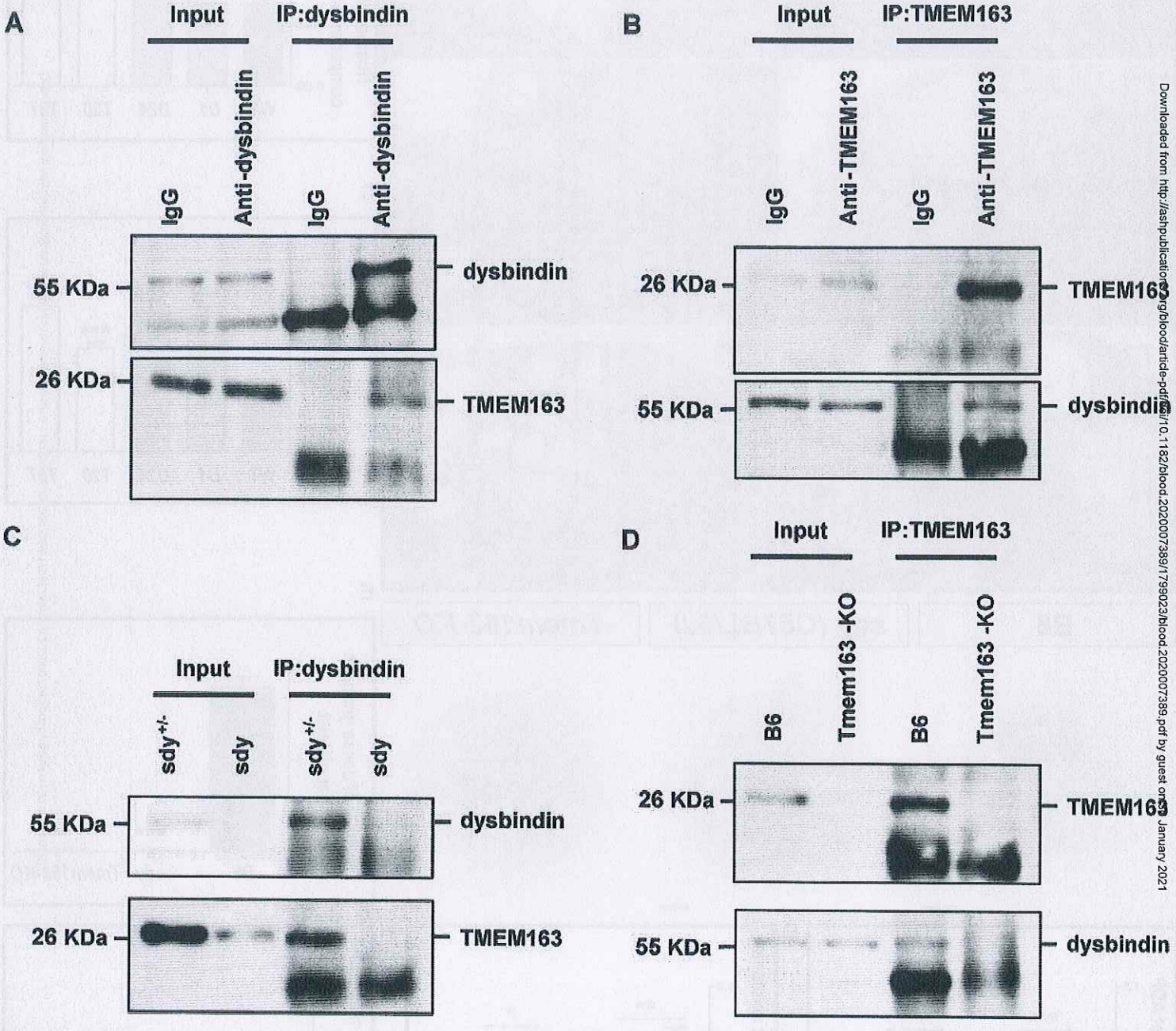
Downloaded from http://ashpublications.org/blood/article-pdf/doi/10.1182/blood.2020007389/1799023/blood.2020007389.pdf by guest on 30 January 2021

Figure 2



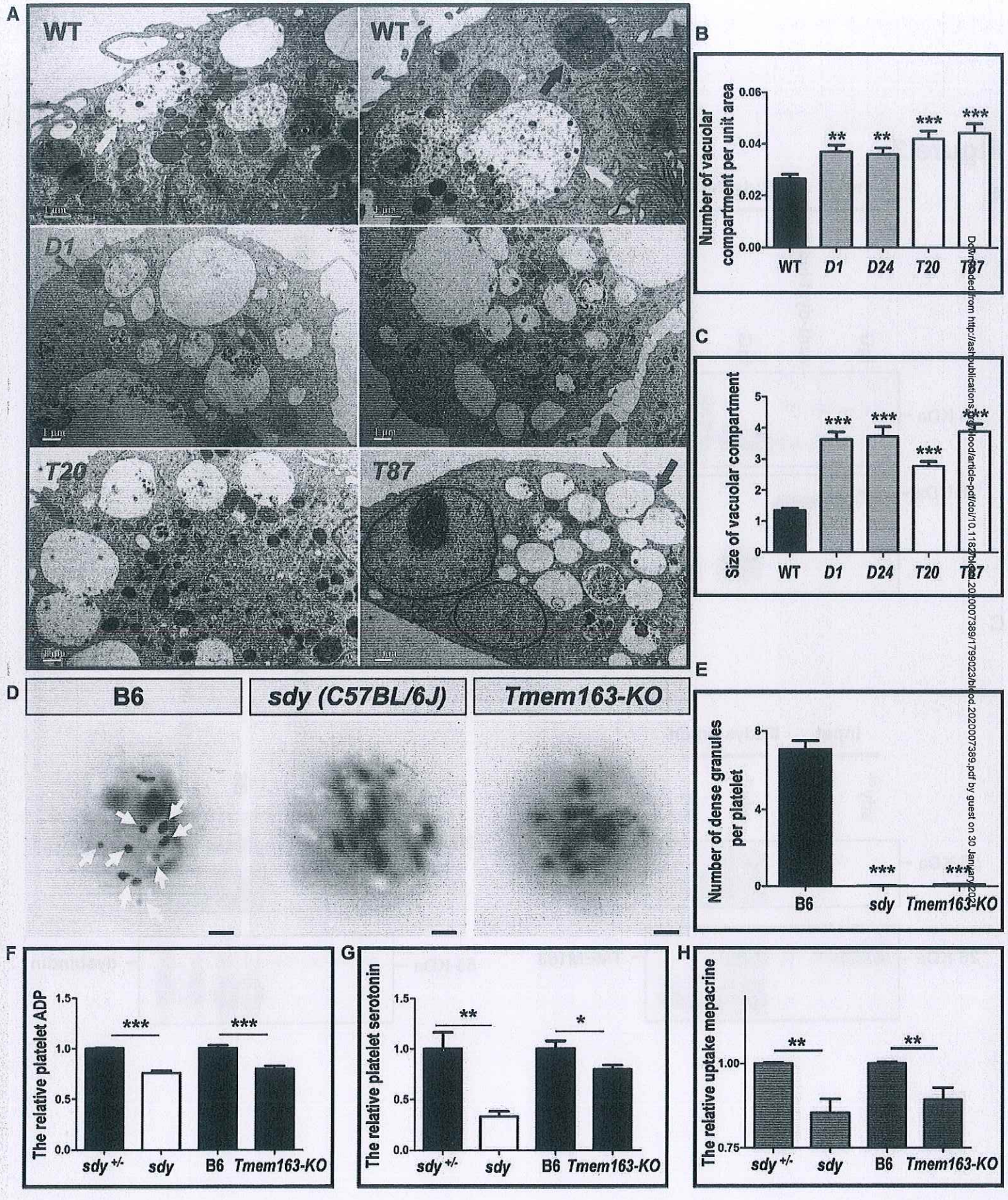
Downloaded from http://ashpublications.org/blood/article-pdf/doi/10.1182/blood.2020007389/1799023/blood.2020007389.pdf by guest on 30 January 2021

Figure 3



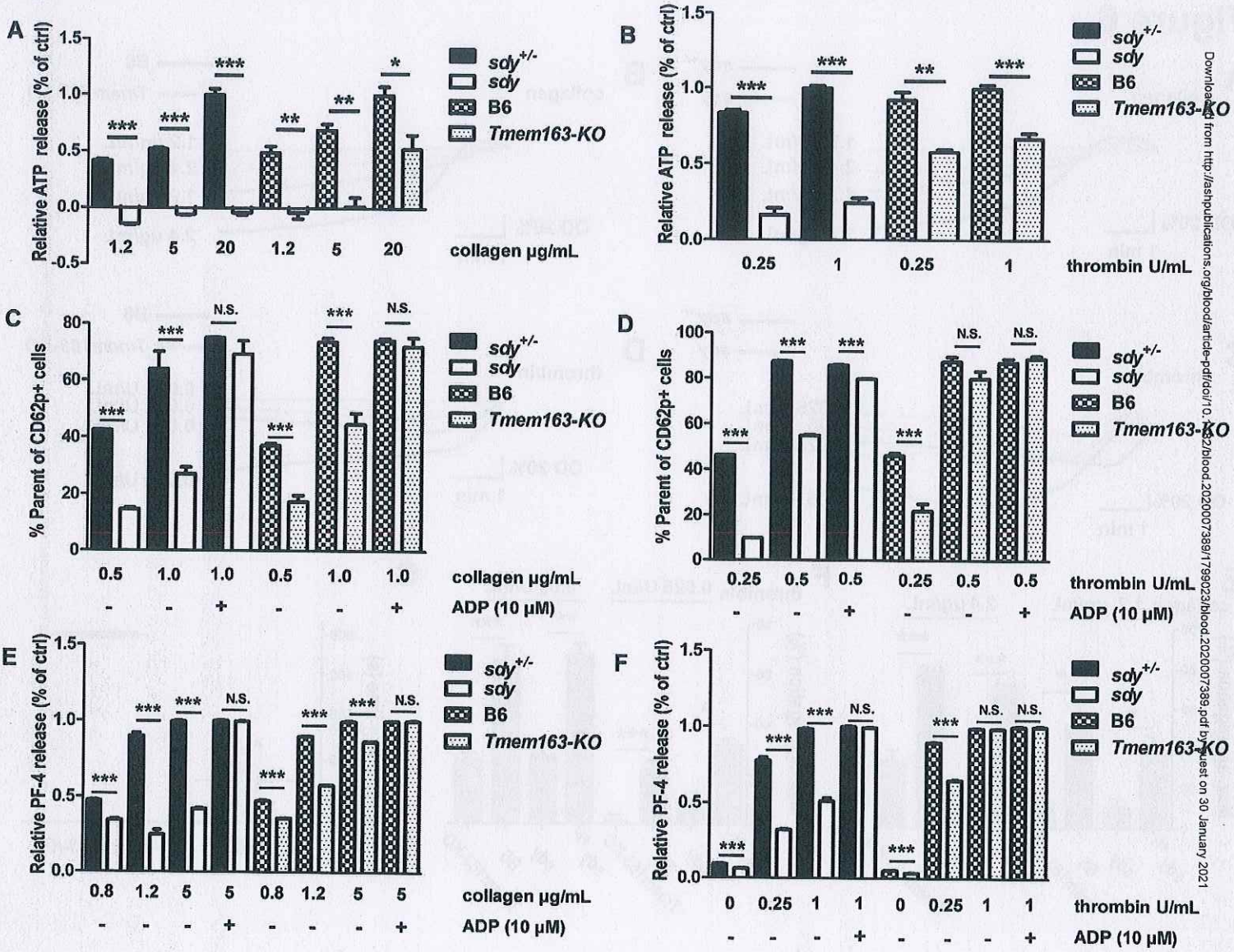
Downloaded from http://ashpublications.org/blood/article-pdf/doi/10.1182/blood.2020007389/1799023/blood.2020007389.pdf by guest on 29 January 2021

Figure 4



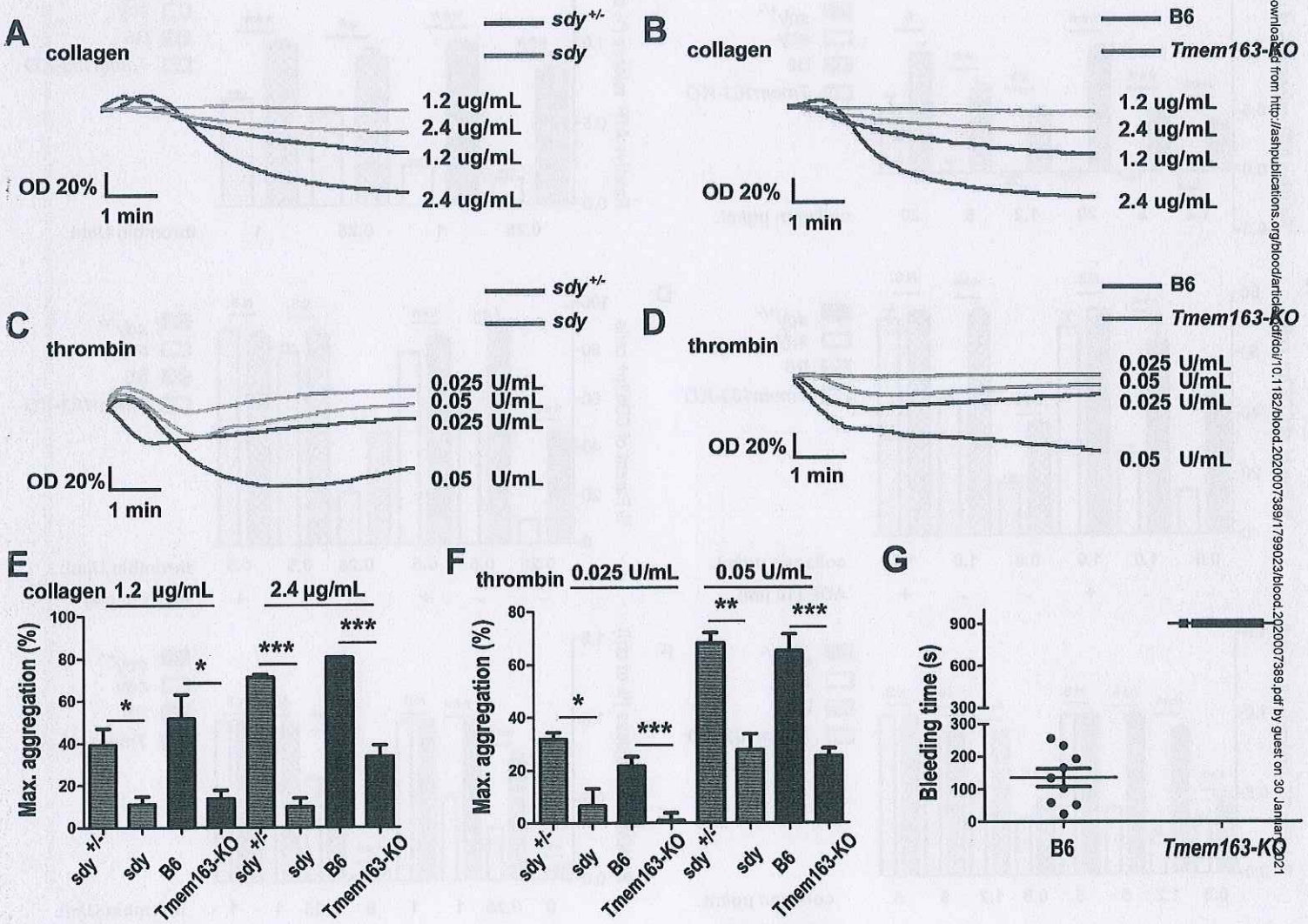
Downloaded from http://ashpublications.org/blood/article-pdf/doi/10.1182/blood.2020007389/1799023/blood.2020007389.pdf by guest on 30 January 2021

Figure 5



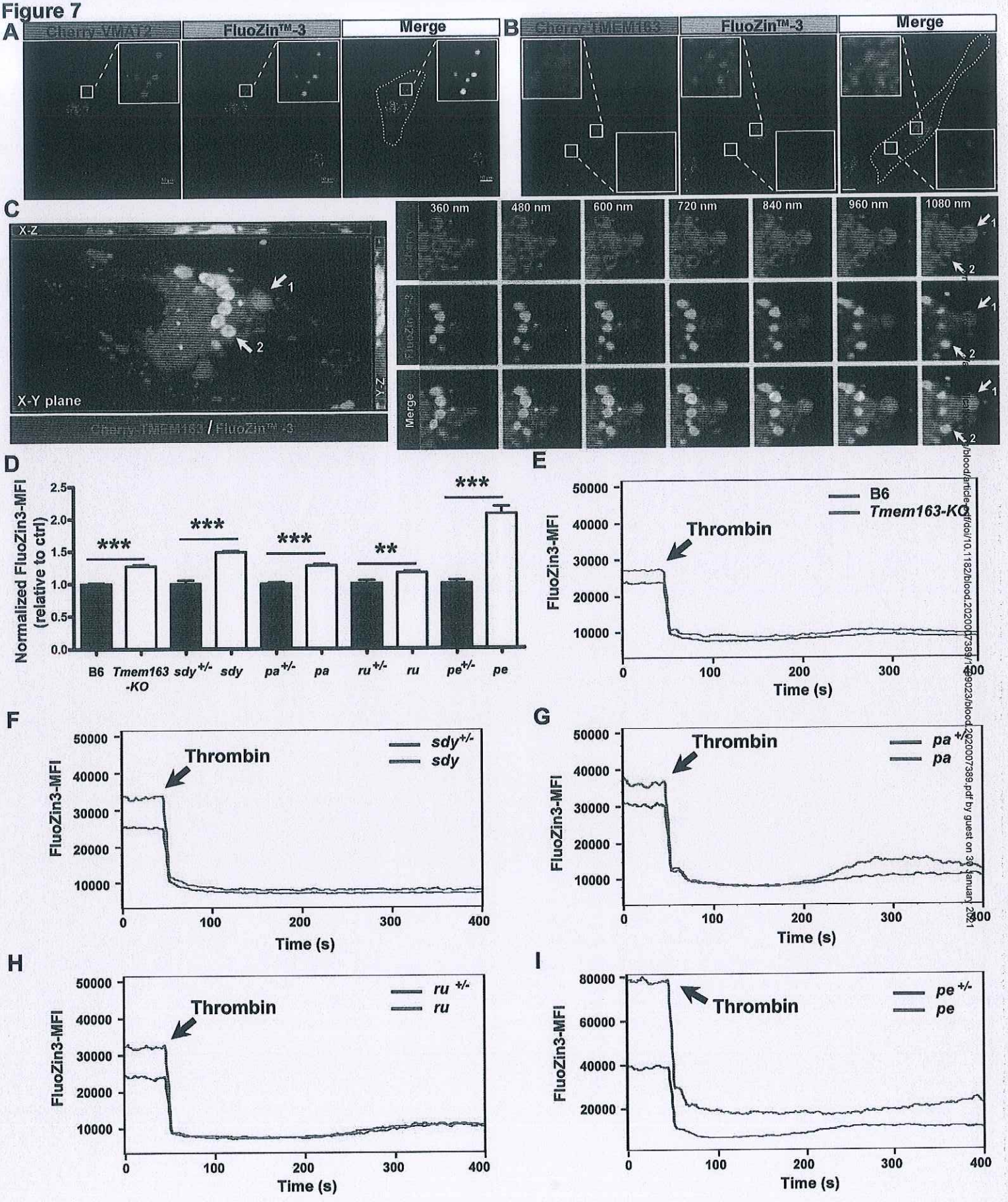
Downloaded from http://ashpublications.org/blood/article-pdf/doi/10.1182/blood.2020007389/1799023/blood.2020007389.pdf by guest on 30 January 2021

Figure 6



Downloaded from http://ashpublications.org/blood/article-pdf/doi/10.1182/blood.2020007389/1799023/blood.2020007389.pdf by guest on 30 January 2021

Figure 7



https://ashpublications.org/blood/article-pdf/doi/10.1182/blood.2020007389/1899023/blood.2020007389.pdf by guest on 30 January 2021